IOP Publishing | International Atomic Energy Agency Nuclear Fusion
Nucl. Fusion **54** (2014) 023004 (9pp) doi:10.1088/0029-5515/54/2/023004

Scaling mechanisms of vapour/plasma shielding from laser-produced plasmas to magnetic fusion regimes

Tatyana Sizyuk and Ahmed Hassanein

Center for Materials under Extreme Environment, School of Nuclear Engineering, Purdue University, West Lafayette, IN 47907, USA

E-mail: tsizyuk@purdue.edu (T. Sizyuk) and hassanein@purdue.edu (A. Hassanein)

Received 20 August 2013, revised 11 December 2013
Accepted for publication 17 December 2013
Published 21 January 2014

Abstract

The plasma shielding effect is a well-known mechanism in laser-produced plasmas (LPPs) reducing laser photon transmission to the target and, as a result, significantly reducing target heating and erosion. The shielding effect is less pronounced at low laser intensities, when low evaporation rate together with vapour/plasma expansion processes prevent establishment of a dense plasma layer above the surface. Plasma shielding also loses its effectiveness at high laser intensities when the formed hot dense plasma plume causes extensive target erosion due to radiation fluxes back to the surface. The magnitude of emitted radiation fluxes from such a plasma is similar to or slightly higher than the laser photon flux in the low shielding regime. Thus, shielding efficiency in LPPs has a peak that depends on the laser beam parameters and the target material. A similar tendency is also expected in other plasma-operating devices such as tokamaks of magnetic fusion energy (MFE) reactors during transient plasma operation and disruptions on chamber walls when deposition of the high-energy transient plasma can cause severe erosion and damage to the plasma-facing and nearby components. A detailed analysis of these abnormal events and their consequences in future power reactors is limited in current tokamak reactors. Predictions for high-power future tokamaks are possible only through comprehensive, time-consuming and rigorous modelling. We developed scaling mechanisms, based on modelling of LPP devices with their typical temporal and spatial scales, to simulate tokamak abnormal operating regimes to study wall erosion, plasma shielding and radiation under MFE reactor conditions. We found an analogy in regimes and results of carbon and tungsten erosion of the divertor surface in ITER-like reactors with erosion due to laser irradiation. Such an approach will allow utilizing validated modelling combined with well-designed and well-diagnosed LPP experimental studies for predicting consequences of plasma instabilities in complex fusion environment, which are of serious concern for successful energy production.

Keywords: MFE, LPP, plasma radiation, plasma shielding

(Some figures may appear in colour only in the online journal)

1. Introduction

Damage and erosion of tokamak plasma-facing and divertor materials and nearby components during plasma instabilities and major disruptions are among the most serious concerns of realizing reliable production of magnetic fusion energy (MFE). Plasma–material interactions and reactor off-normal operating regimes, which plasma-facing components (PFCs) can withstand, were extensively studied during recent years [1–4]. These studies determined the main mechanisms of material erosion during major plasma instabilities and estimated surface erosion for various transient events, resulting in short intense energy loads, corresponding to disruptive plasma instabilities, edge-localized modes (ELMs) or vertical displacement events (VDEs) due to the loss of plasma confinement. In addition to the destruction of PFCs, losses of wall and divertor materials can increase core plasma contamination and further affect plasma confinement. The results highlighted the importance of accurate multi-dimensional and multi-physics modelling and simulations since consequences of these events require integrated analysis of complex physical processes in a realistic three-dimensional (3D) reactor design.

High intensity of power deposition during these events results in a rapid increase in the surface temperature, material melting and erosion, and vapour plasma formation from the eroded material that subsequently causes different and complex mechanisms of plasma–material surface interactions such as vapour/plasma shielding and resulting radiation effects, plasma interaction with the melt layer, and evolution of

 © 2014 IAEA, Vienna Printed in the UK

liquid droplet formation and splashing. These processes require self-consistent multi-physics approaches in modelling of such events taking into account various energy dissipation mechanisms and the influence of these processes on material behaviour and plasma evolution. For example, recent integrated modelling, considering the entire area of tokamak divertor, showed significant effect of a plasma shielding layer on surface erosion at the strike point of high energy load as well as strong radiation from the shielding layer to the nearby components [5]. Investigation of this problem in the current fusion devices is restricted due to the lack of sufficient power. Comprehensive and complex experiments with accurate measurement and diagnostic techniques are required for reliable predictions. From the point of view of future fusion reactors, the importance of accurate analysis is significant because of the planned higher operating power and, therefore, significantly increasing potential damage and failure of plasma-facing as well as nearby components.

Precise analysis of material erosion and plasma shielding effects can be carried out utilizing well-designed yet simple laser-produced plasma (LPP) experiments coupled with well-benchmarked modelling. Integrated self-consistent modelling with accurate description of all processes involved and having multi-dimensional configuration can be used for the predictions and for design of experiments to be conducted in parallel with computer simulations. Such an integrated approach, concurrent experimental and modelling research, will allow excluding possible uncertainties and further predict tendencies for extrapolated wider range of parameters and regimes expected in future power reactors.

Our HEIGHTS (High Energy Interaction with General Heterogeneous Target Systems) package is designed for detailed simulation of LPPs. The HEIGHTS package includes models for 3D description of energy deposition, vapour/plasma shielding cloud formation/evolution and magnetohydrodynamic (MHD) processes, thermal conduction in material and in plasma, atomic physics processes and resulting opacities, detailed photon radiation transport (RT), and the interaction between the plasma/radiation and the target material. We extensively benchmarked and utilized the package in modelling and optimization of LPP sources for extreme ultraviolet (EUV) lithography, the current leading method for the manufacturing of next-generation computer chips [6, 7]. We considered several lasers, materials and target configurations to develop efficient sources for EUV photon production. In the processes of optimization, the shielding effect of the plasma produced from small liquid tin droplets (leading target material for EUV production) and the resulting EUV source performance were investigated in great detail [7]. For example, we studied the effect of various laser parameters and wavelengths on the conversion efficiency (EUV photon yield versus incident laser energy) of such devices and found that CO_2 lasers having a longer wavelength, regardless of pulse intensity have several advantages over Nd : YAG lasers. The shielding effect also explained the higher conversion efficiency of dual-beam LPP sources when a Nd : YAG laser with a shorter wavelength was used for pre-plasma production followed by CO_2 laser heating of this optically thin pre-plasma for efficient EUV photon generation.

In this work, we studied the shielding effect in LPPs of carbon and tungsten targets. These materials are considered as the main coating materials of PFCs in tokamaks in the areas where intense heat fluxes from the disruptive plasma are expected. In spite of the differences in time scales, energy source and intensities of transient events between MFE reactors and nanosecond laser devices we found an analogy in plasma evolution, conversion of source energy to radiation and shielding efficiency among these systems. Taking into account the relative simplicity and well-controlled laser devices for accurate modelling and precise measurements compared with the complex fusion reactors, such an approach can be used for the investigation of various materials and compounds with regard to the erosion dynamics, shielding efficiency, components lifetime, radiation to nearby components and potential chamber contamination issues in a much cheaper and significantly faster way.

The plasma temperature and density given in the paper correspond to electron temperature and density.

2. HEIGHTS model description

Modelling material ablation and plasma production by lasers was performed utilizing the HEIGHTS package. A detailed description of models, different approaches, comprehensive analysis of methods and results of benchmarking of the package can be found elsewhere [8, 9]. HEIGHTS is a very versatile and flexible package, in terms of target materials, target geometry, input source energy, i.e. laser parameters, and is tuned for accurate modelling of all main processes occurring in nanosecond laser devices in the range of 10^8–10^{13} W cm^{-2} power densities. The processes of laser photon absorption and reflection, target heating and vaporization, vapour plume expansion and ionization, electron and ion interaction, thermal and radiation energy dissipation are modelled self-consistently in full 3D geometry. Our modelling analysis showed that multi-dimensional description of LPP processes further reveals the integrated character of these processes and their interplays in LPP devices.

HEIGHTS employs splitting methods, calculating the evolution of plasma/vapour hydrodynamics and using energy dissipation due to thermal conduction and RT as correction factors for the results of the predicted convection fluxes. The energy distribution in domain is considered separately for ions and electrons. Monte Carlo modelling of laser energy deposition takes into account laser photon interaction with a solid/liquid target, with vapour and plasma including photon absorption, reflection and reabsorption after reflection [8, 10]. These processes interplay with target thermodynamics evolution, vapour/plasma plume thermo- and hydrodynamics, and plasma radiation. Our analysis and simulations of LPP devices showed the importance of integrated self-consistent modelling of all processes involved in benchmarking actual experiments and LPP devices [7]. Modelling of target evaporation considers detailed kinetic processes on the target surface and takes into account the possibility of recondensation [11]. The process of correct conversion of laser energy to plasma radiation is very important in the accurate simulation of LPPs. The models and methods used for the description of energy transport in a plasma by radiation fluxes can significantly affect the simulation results. We considered and have implemented two different approaches for modelling

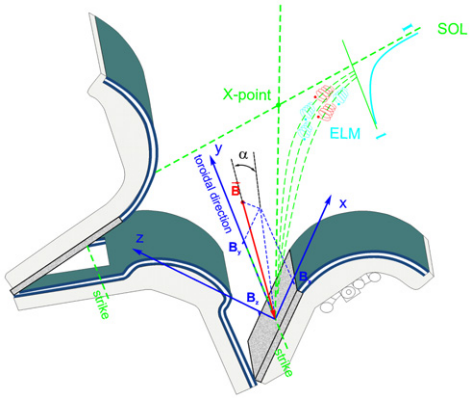

Figure 1. Schematic illustration of ITER-like divertor design and coordinate systems used in HEIGHTS modelling [16]. Angle α corresponds to the poloidal angle of magnetic field lines at the divertor surface in tokamak reactors.

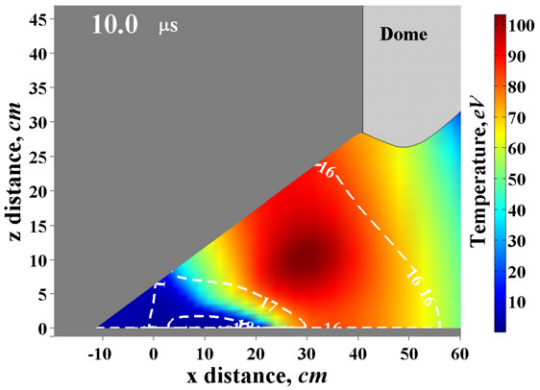

Figure 2. Electron temperature and density (white contours) distribution in the vapour/plasma plume developed from eroded carbon during the first 10 μs of disruption.

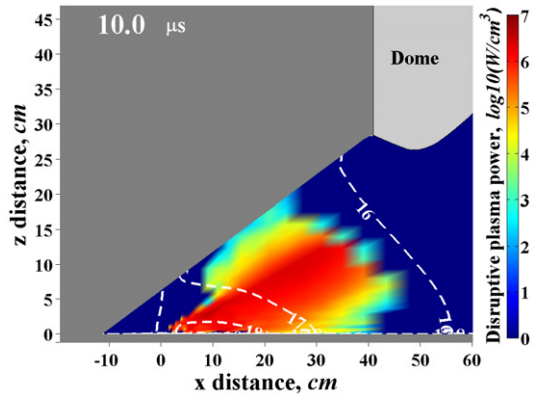

Figure 3. Disruptive plasma power and electron density (white contours) distribution in the vapour/plasma plume developed from eroded carbon during the first 10 μs of disruption.

of RT: a direct numerical solution of the RT equation using the Gaussian quadrature method for volume integration along the path of photons and Monte Carlo models with several weighting factors to enhance accuracy and reduce the extensive computational time required for the simulation [8]. These models were verified and benchmarked within our analysis for optimization of plasma sources for EUV lithography [12, 13]. Plasma thermodynamic properties and optical coefficients are calculated using the self-consistent Hartree–Fock–Slater (HFS) model implemented in HEIGHTS [14]. The populations of atomic levels, ionization balance, and the ion and electron plasma concentrations are obtained based on the collisional–radiative equilibrium (CRE) approximation. Tabulated plasma properties and optical coefficients for a wide range of temperatures and densities are used during the simulation of the whole cycle of plasma evolution in the LPP.

3. Vapour shielding in magnetic fusion

Modelling results of plasma instabilities during ELMs and disruptions, with anticipated ITER parameters, showed that the initial layer of evaporated carbon from the divertor surface can reduce the plasma heat flux to the surface by more than 20 times protecting, thereby, the divertor surface from further high erosion and damage [5, 15]. For ITER disruption scenarios, with 126 MJ total impact energy (100% pedestal energy) on the carbon divertor plate, the maximum unshielded energy density of 5 kJ cm^{-2} could result in the evaporation of ~200 μm of carbon layer at the strike point. However, the vapour layer formed above the strike point during the first 5–10 μs of disruption leads to absorption and redistribution of core plasma energy and significant protection of the surface from further erosion that results in reducing the erosion depth by ~1000 times in comparison with unshielded scenarios.

Figure 1 shows a schematic description of the ITER-like divertor area and illustrates plasma particle transport to the divertor surface during plasma instability events such as ELMs and disruptions. This configuration was used in our modelling analysis of divertor surface response to these events [16].

An analysis of vapour/plasma characteristics in the developed plume from the divertor eroded carbon showed that a plume with plasma density of the order of 10^{18} cm^{-3} and thickness of 1–2 cm can be formed during the first 10 μs, as shown in figure 2. Based on cross-sections for interactions of D/T/electrons with such a vapour/plasma plume we estimated that the incident 3.5 keV D/T ions will totally lose their energy in the 0.2–0.3 cm layer and the intensity of the incident core plasma electrons will also significantly slow down in their way through the developed plasma. Figure 3 shows absorption of disrupting plasma energy in the developed plume above the divertor surface that resulted in reducing heat intensity to the divertor strike area and protection of the surface at this location.

The early development of a protective layer during very short time was possible due to the high evaporation rate of the carbon surface caused by the initial intense heat flux of 50 MW cm^{-2} and high velocity of the developed hot plume. A plume with a velocity of 1–10 km s^{-1} can expand up to 0.1–1 cm during 1 μs, as shown in figure 4.

However, such a hot plasma with temperatures up to 120 eV (still much lower than the original disrupting plasma temperature) caused extensive erosion of surfaces surrounding the strike point. Radiation fluxes from the carbon plasma with intensity of the order of 10^6 W cm^{-2} to the divertor during a disruption time of 100 μs were the main reason for the erosion along 40 cm of the divertor surface [5, 17]. The radiation energy density to surfaces of nearby components was even

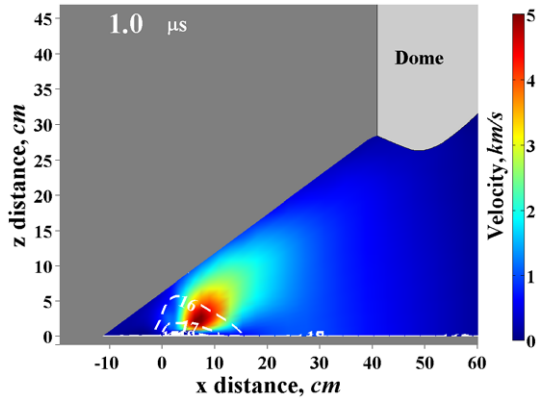

Figure 4. Electron density (white contours) distribution and velocity in the vapour/plasma plume developed from eroded carbon during first 1 μs of disruption.

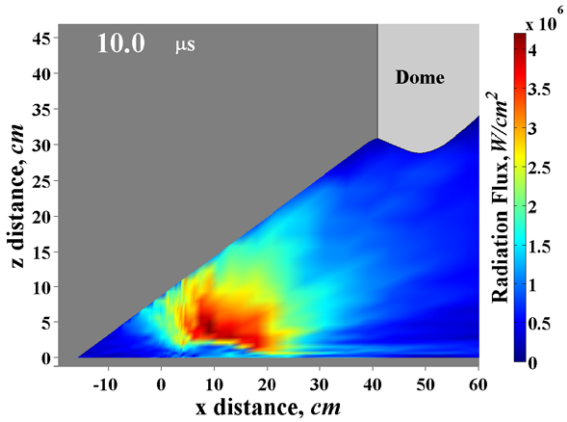

Figure 5. Radiation fluxes in the plasma developed from eroded carbon.

higher. Such potential damage of nearby components has to be evaluated very carefully when choosing plasma-facing and nearby materials as well as divertor design and configuration in future power reactors [1]. Figure 5 shows radiation fluxes in the carbon plasma as well as illustrates surfaces in the divertor area subjected to plasma radiation with such high intensities.

The above example showed the importance of thorough analysis of materials as candidates for the divertor surface coating to predict erosion of these materials during plasma instabilities as well as to predict potential damage resulting from the secondary plasma developed from the eroded material. Estimation of vapour/plasma shielding efficiency and magnitude of plasma radiation fluxes can be predicted through a detailed analysis of material behaviour using simple and well-diagnosed LPP devices.

4. Prediction of similar conditions in LPP

Based on the main characteristics of disruption energy load used in our analysis for ITER-like conditions such as maximum unshielded energy density of 5 kJ cm^{-2} deposited during 100 μs we estimated the initial parameters of a laser beam needed to simulate carbon erosion and shielding efficiency in LPP devices. Taking into account a typical Nd : YAG laser pulse duration of 10 ns, that is four orders of magnitude lower than a tokamak plasma disruption duration, we predicted 5×10^{11} W cm^{-2} for the laser beam intensity.

Spot size is another important parameter of a laser beam that can influence target erosion and developed plasma characteristics. Figures 6(*a*) and (*b*) show the difference in plasma temperature and mass density distribution in a plasma created by lasers with 100 μm and 300 μm spot sizes, respectively, using the above laser beam intensity and duration. In both cases craters with the same depth of around 1 μm were created, as shown in figures 7(*a*) and (*b*). The main difference is in the larger volume of material eroded by the laser with a larger spot size that resulted in a higher plasma density in the plume. Higher absorption of laser photons as well as slower processes of plasma cooling by radiation transport and by energy dissipation due to thermal conduction in such a dense plasma explain the higher temperatures shown in figure 6(*b*).

The optically thick plasma plume developed during laser irradiation protected the target surface from laser photons that significantly decreased target erosion. However, the high intensity of radiation fluxes from the hot and dense plasma reduced the shielding efficiency for the considered laser intensity. Plasma radiation was the main energy source that caused extensive evaporation and determined the spatial temperature profiles in the target. Figures 8(*a*) and (*b*) show the shielding efficiency of plasma plumes in both cases demonstrating almost total protection of the target from the incident laser irradiation at the centre of the laser spot, however, predicting high energy density of plasma irradiation to the target at this location. The combined effect of low shielding from laser photons and radiation fluxes from peripheral plasma regions is the reason for intensive evaporation of the target at the borders of the laser spot area that is more evident in the case of a larger spot size (figure 7(*b*)).

Figures 8(*a*) and (*b*) clearly demonstrate the processes developed above the surface during laser interaction with the target and with the evolving plasma. Heating and evaporation of the target, flow of vapour/plasma from the crater, and, at the same time, compression of the plasma plume at the laser spot centre resulted in variation of the plasma layer thickness above the surface during laser irradiation that influenced surface protection and shielding efficiency. Due to the large difference in energy transfer to the target in the spot area and outside as well as due to low thermal conductivity in carbon, sharp boundaries in temperature profiles are seen in figure 7(*b*). The difference in the shown spatial dimensions, i.e. several hundreds of micrometres along the surface and up to 2 μm in depth, increases visual evidence of such boundaries.

In spite of similar temperature ranges in the plasma developed during disruption in the fusion reactor environment and in LPP devices using a Nd : YAG laser, the denser plasma plume created by this laser resulted in almost four orders of magnitude larger radiation fluxes from such a plasma to the target. Taking into account the difference in time scale between the considered events, the total energy density from plasma radiation to the target at the centre of the beam spot can be the same as that at the location of the maximum unshielded energy density on the divertor surface [5]. Since plasma irradiation was the main source of target erosion in both cases, similarity in shielding and erosion mechanisms in MFE and LPP devices is evident. Thus, one can find an analogy in the processes

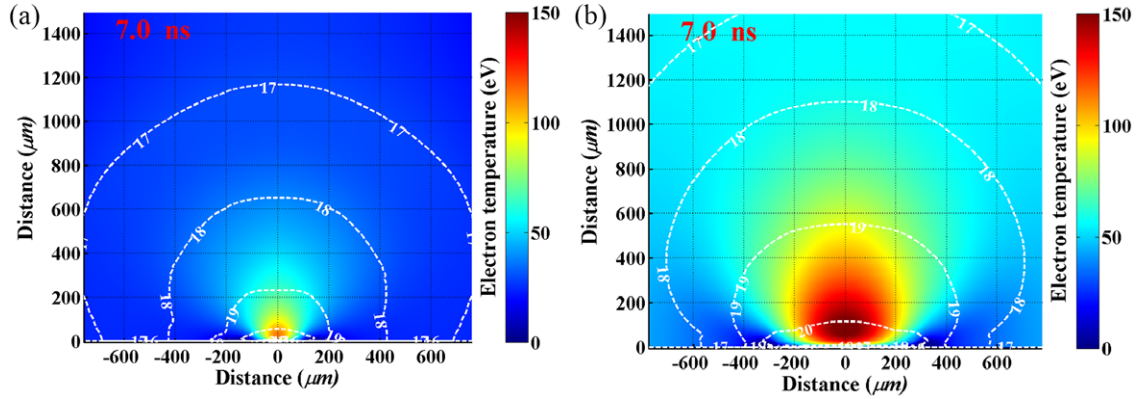

Figure 6. Electron temperature and density (white contours) distribution in the vapour/plasma plume developed from the carbon target by a Nd : YAG laser with (*a*) 100 μm and (*b*) 300 μm spot sizes.

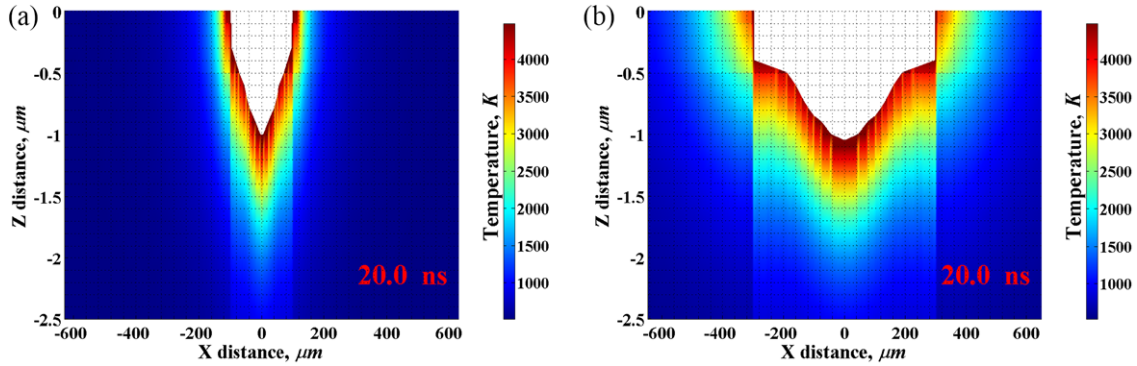

Figure 7. Carbon erosion by a Nd : YAG laser with (*a*) 100 μm and (*b*) 300 μm spots and 5×10^{11} W cm^{-2} intensity.

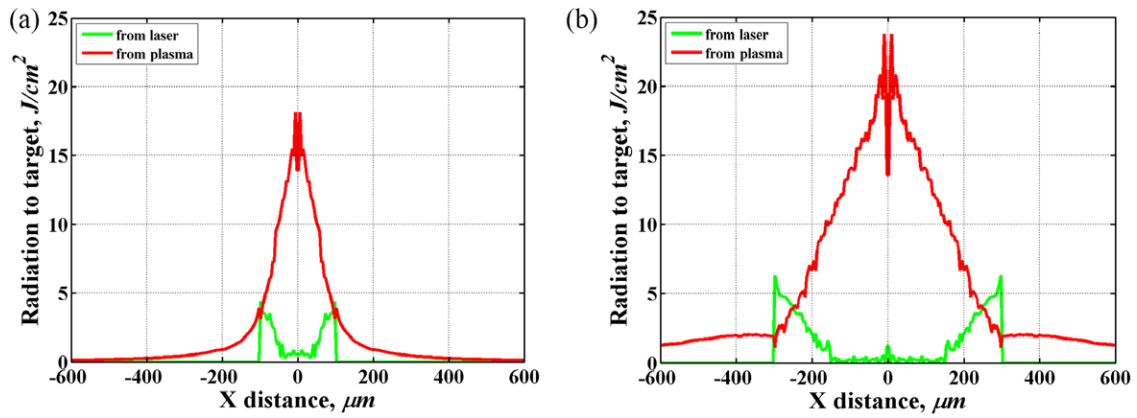

Figure 8. Energy density to the target from the laser and from the developed plasma for (*a*) 100 μm and (*b*) 300 μm spot sizes of Nd : YAG laser beams.

of target erosion from the two different initial energy sources such as core plasma particles in MFE and laser photons in LPP devices and by the secondary, created source–radiation fluxes from the developed plasma of the eroded material.

To further track the dependence of shielding efficiency on the energy density in different devices we simulated carbon ablation by a laser beam with ten times lower intensity that, based on our scaling mechanism, can correspond to a giant ELM energy load during 100 μs in ITER-like devices [15]. Figures 9 and 10 show that the developed secondary vapour plasma also had the same temperature range in both MFE and LPP environments. Similar to the more intensive disruptive regimes described above, radiation fluxes to the target were also approximately four orders of magnitude higher in the LPP device due to the denser plasma developed.

Because of this lower intensity of energy sources in both LPP and MFE cases, and therefore lower evaporation rate, a less dense and colder plasma was created. Hence, the shielding efficiency from the main source particles was significantly reduced in comparison with the previous higher intensity regimes. The erosion of the target in this case was mainly due to ions and electrons in the MFE device [5] and by laser photons in the LPP rather than radiation fluxes from the developed shielding layer. Crater depths on the divertor surface as well

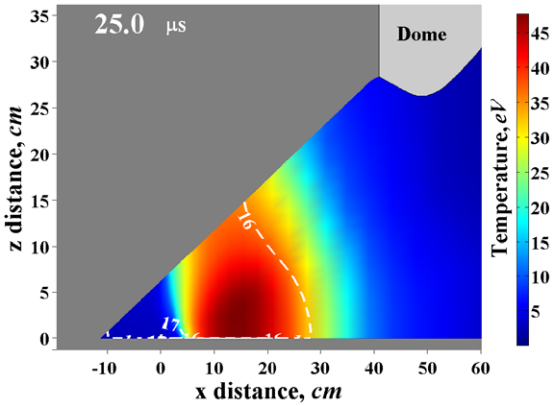

Figure 9. Electron temperature and density (white contours) distribution in the vapour/plasma plume developed from eroded carbon during the first 25 μs of the giant ELM with 100 μs duration.

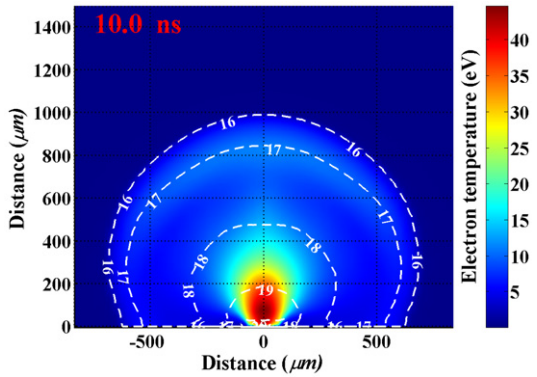

Figure 10. Electron temperature and density (white contours) distribution in the vapour/plasma plume developed from the carbon target by a Nd : YAG laser with 100 μm spot and 5×10^{10} W cm^{-2} intensity.

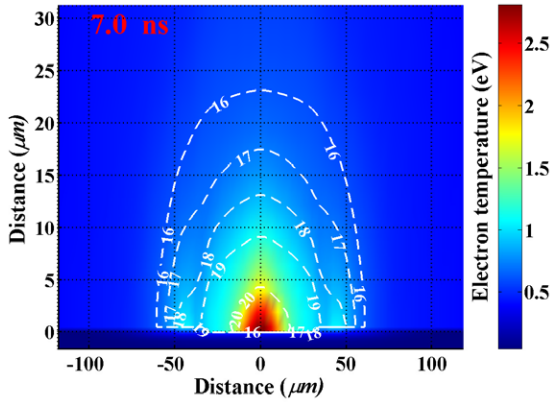

Figure 11. Temperature and density (white contours) distribution in the plasma plume developed from the W target by a Nd : YAG laser with 100 μm spot and 1×10^9 W cm^{-2} intensity.

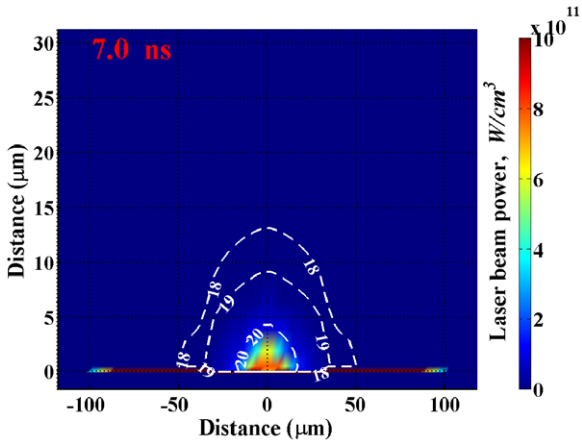

Figure 12. Laser beam power distribution in the developed plasma.

as on the carbon plate in the LPP device were approximately two times lower in this case for ten times lower intensities of these events. Relevant scaling can be easily developed and benchmarked using simple LPP experiments and simulations.

5. Vapour/plasma shielding in the LPP

We studied the effect of vapour shielding and plasma radiation on target ablation for two materials, i.e. low-Z carbon and high-Z tungsten, by varying several laser beam parameters. The pulse intensity of the laser beam for a given wavelength is one of the main parameters in determining plasma temperatures and density distribution. Other parameters such as the pulse duration, shape and spot size also affect the range of values and combination of these characteristics. However, the tendency in target ablation shape and the main energy source responsible for the ablation, i.e. laser photons or plume plasma photons, are determined by the laser intensity.

Initially, we found the lowest reasonable intensity of the laser beam for tungsten erosion based on the estimation of the lowest energy density required for vaporization of a significant amount of material to get a tangible plasma layer with temperatures around 1 eV and higher. From tungsten thermodynamic properties, about 1 J cm^{-2} is required for heating the material up to its boiling point and for further vaporization of a layer of about 100 nm. Taking into account the reflectivity of the Nd : YAG laser with 1064 nm wavelength from the W surface [18] as well as the energy distribution due to high thermal conductivity in this material even for nanosecond time duration, we estimated the lowest energy density to be 3–4 J cm^{-2}. We started simulations utilizing 5 J cm^{-2} with typical laser beam duration for a Nd : YAG laser, e.g. 5 ns, that leads to 1 GW cm^{-2} intensity. We obtained in modelling a maximum ablation depth of $\sim$100 nm. Our simulations showed that the erosion of the target was caused mainly by laser photons and only half of the laser energy at the spot centre was transferred to the target that demonstrates the shielding effect of the tungsten vapour/plasma even at such a low beam intensity.

Figures 11 and 12 demonstrate the processes of plasma evolution at the end of the laser pulse and the corresponding location of preferential laser energy absorption in the developed plume. These results for plasma evolution in W at a low laser intensity are consistent with results for energy density threshold for laser-induced plasma formation in tungsten obtained in experiments [18].

Based on the above benchmarking of the start point for modelling of tungsten ablation by a laser beam we extended

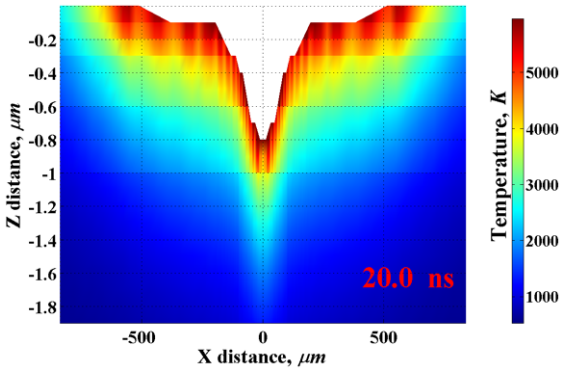

Figure 13. Tungsten erosion by a Nd : YAG laser with 100 μm spot, 10^{12} W cm^{-2} intensity and 10 ns pulse.

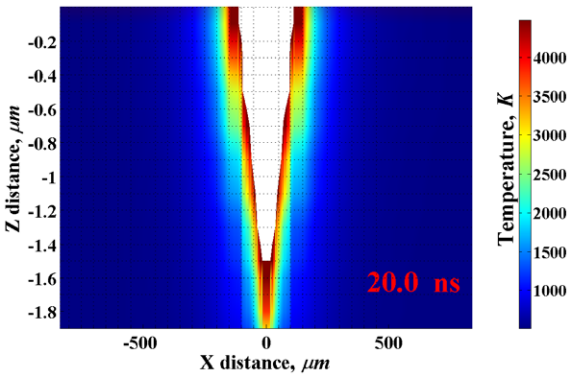

Figure 14. Carbon erosion by a Nd : YAG laser with 100 μm spot, 10^{12} W cm^{-2} intensity and 10 ns pulse.

the range of considered intensities up to 10^{12} W cm^{-2}, as shown in figures 13 and 14 for both tungsten and carbon targets.

For higher laser intensities, the shape of the crater or the evaporated mass is the most important characteristic in the analysis of target ablation and shielding effect, rather than the crater depth as usually analysed in experiments. For example, figures 13 and 14 show that the laser with an intensity of 10^{12} W cm^{-2} creates an almost two times deeper crater in carbon than in tungsten. However, the width of the crater in the W sample is several times larger and significantly exceeds the laser spot size. The intense radiation flux from the plasma developed from the high-Z material is one of the reasons for that. Although the vaporized layer of the high-Z material provides higher protection of the target from laser photons, it generates ten times higher radiation fluxes from the developed plasma, as shown in figures 15 and 16. Radiation fluxes that caused intense evaporation of the target surface in the original spot area had also large effects on nearby surfaces. This should be taken into account in the analysis of materials and reactor design for MFE environment.

Figures 17 and 18 show the difference in shielding efficiency of tungsten and carbon plasmas at the crater centre developed by the Nd : YAG laser with the same beam parameters. The evaporated mass and maximum crater depth in the carbon target did not change significantly (0.3–0.5 μm) up to 10^{11} W cm^{-2} laser intensity that corresponds to approximately the same total energy load due to low shielding by the carbon plasma and low irradiation from

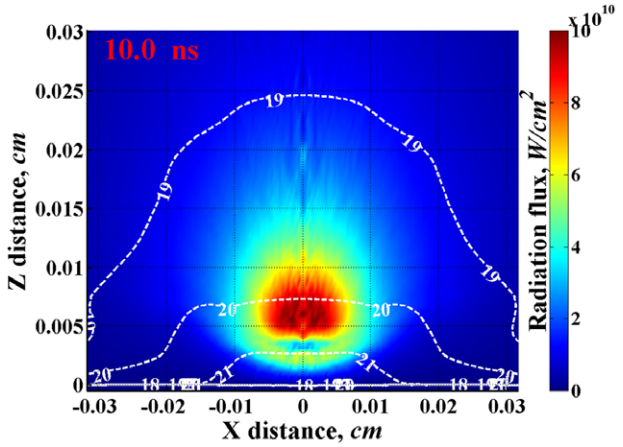

Figure 15. Radiation fluxes and plasma density (white contours) in the W plasma produced by a Nd : YAG laser with 100 μm spot, 10^{12} W cm^{-2} intensity and 10 ns pulse.

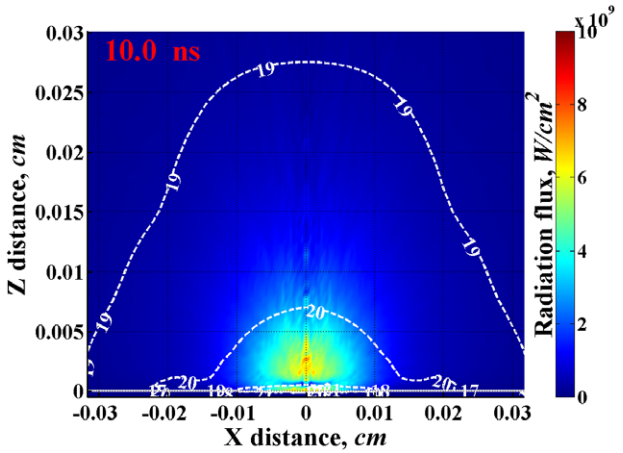

Figure 16. Radiation fluxes and plasma density (white contours) in the C plasma produced by a Nd : YAG laser with 100 μm spot, 10^{12} W cm^{-2} intensity and 10 ns pulse.

the plasma (figure 18). We should note that these results are consistent with experimental measurements of plasma parameters at 3 mm distance from the carbon sample where almost steady-state temperature and density values were found in the range of laser intensities from 10^{10} to 10^{11} W cm^{-2} [19].

Better protection of the surface at the spot centre from laser irradiation as well as from hot plasma irradiation by the denser tungsten vapour/plasma plume results in almost two times less erosion depth of the developed crater (figure 17). However, the tungsten target received almost ten times more of the total energy at higher laser beam intensities compared with carbon, as shown in figures 19 and 20. The evaporation rate from tungsten was totally determined by the high radiation from the plasma, as shown in figure 19.

Figures 21 and 22 demonstrate the differences in tungsten and carbon erosion thickness and profile for two laser beam intensities, i.e. 5×10^{10} and 5×10^{11} W cm^{-2}. It was previously shown that a ten times increase in the intensity of core particles in the fusion reactor, corresponding to an increase in energy load during ELM and disruption, results in only two times larger erosion depth on the divertor surface [5]. Carbon erosion

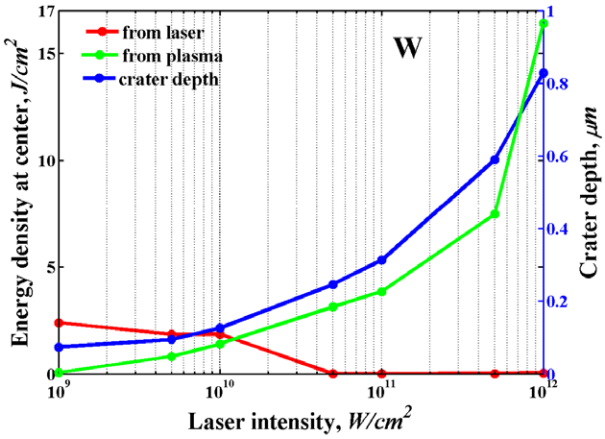

Figure 17. Energy density from the laser and from the plasma at the crater centre of the W target and related crater depth.

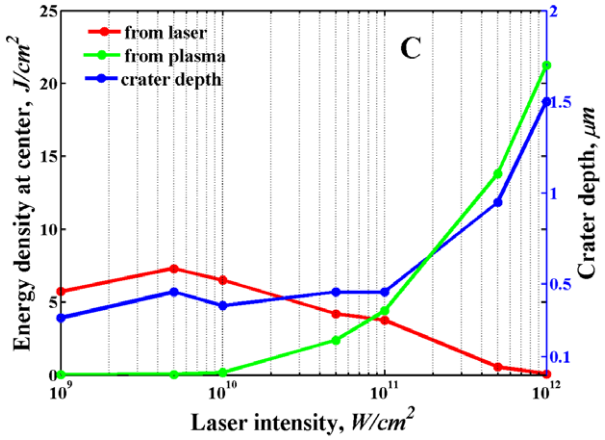

Figure 18. Energy density from the laser and from the plasma at the crater centre of the C target and related crater depth.

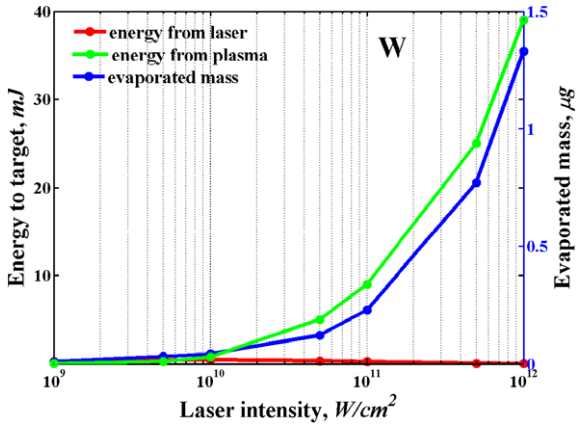

Figure 19. Energy deposition on the W target from the incident laser radiation and from the evolving plasma and the resulting evaporated mass.

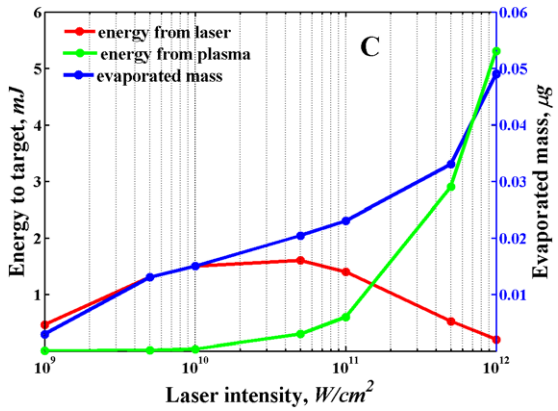

Figure 20. Energy deposition on the C target from the incident laser radiation and from the evolving plasma and the resulting evaporated mass.

in the LPP device shows a similar tendency in the dependence of the crater depth on laser intensity (figure 22). The broader crater in the tungsten target even at a relatively low laser beam intensity is attributed to the high radiation from the tungsten developed plasma, as shown in figure 21.

6. Application of LPP for shielding analysis in MFE

The above results of comparative analysis of plasmas created from solid targets in MFE and LPP devices showed the potential application of simple and well-diagnosed laser experiments to study material erosion and shielding efficiency. The analysis showed the possibility of extrapolating the results to the intensities and time scales relevant to a MFE reactor during major plasma instabilities. Effects of strong radiation from the shielding plasma on secondary nearby components can be predicted based on an analysis of plasma radiation in LPP devices. Several laser beam parameters such as the beam intensity, spot size and pulse duration can be used and adjusted to study through modelling and simple experiments to predict the behaviour of various materials under different extreme conditions. The effect of laser wavelength as well as the number of laser beam shots on crater formation [20], evaporated mass and material modification should also be considered in detail in relation to understanding the effect of various plasma instabilities on PFCs in tokamaks. Further assessment of various mechanisms and processes in MFE environment such as the strong oblique magnetic field will require more comprehensive 3D modelling of LPP devices. We are currently investigating these effects. Comprehensive modelling of reactor environment during plasma instabilities and target ablation using LPP devices with adjusted parameters can help in predicting material damage and lifetime from direct plasma energy deposition as well as from plasma radiation of the shielding layer.

7. Conclusion

Laser beams can be used with adjusted parameters to study through modelling and well-diagnosed simple experiments to predict material behaviour and lifetime under extreme conditions anticipated in magnetic fusion energy (MFE) systems. We developed and implemented a scaling mechanism, from LPP to MFE regimes, to study wall erosion, plasma shielding and radiation under MFE reactor conditions, based on modelling of LPP devices using their typical temporal and spatial scales. In spite of the large differences in time scales, energy source, and intensities of transient events

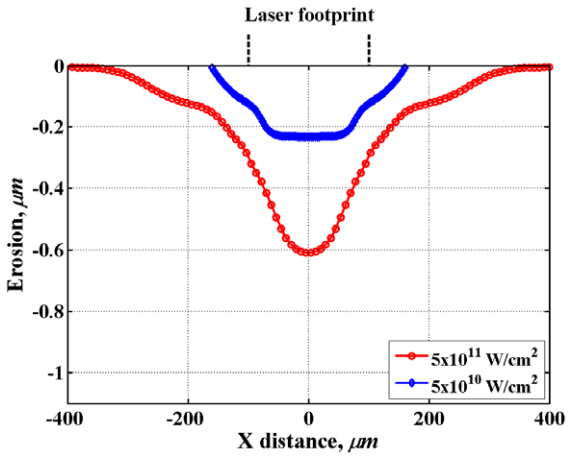

Figure 21. Crater depth and shape in the W target created by a Nd : YAG laser with 100 μm spot, 10 ns pulse, and 5×10^{10} and 5×10^{11} W cm^{-2} intensities.

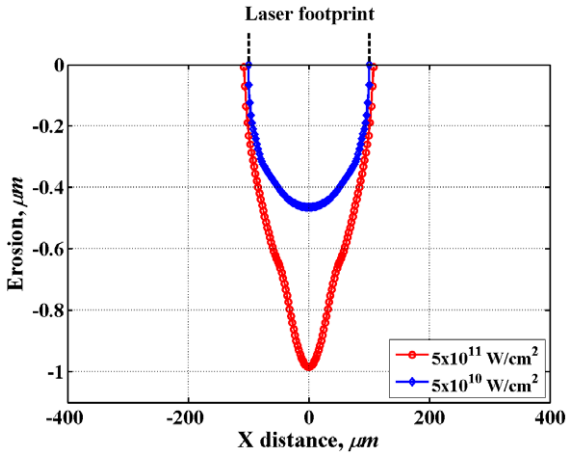

Figure 22. Crater depth and shape in the C target created by a Nd : YAG laser with 100 μm spot, 10 ns pulse, and 5×10^{10} and 5×10^{11} W cm^{-2} intensities.

between MFE reactors and nanosecond laser devices we found an analogy in plasma evolution and shielding efficiency among these systems. Such an approach will allow utilizing validated modelling and well-designed simple experimental studies of LPPs for predictions of damage of plasma-facing and nearby components in MFE environment due to both incident plasma energy as well as radiation of a shielding layer developed during plasma instabilities.

Acknowledgments

This work is partially supported by the National Science Foundation, PIRE project and the US Department of Energy, Office of Fusion Energy Sciences. The authors gratefully acknowledge the computing resources provided by the Fusion cluster operated by the Laboratory Computing Resource Center at Argonne National Laboratory.

References

[1] Hassanein A. 2002 *Fusion Eng. Des.* **60** 527
[2] Federici G. *et al* 2001 *Nucl. Fusion.* **41** 1967
[3] Federici G., Loarte A. and Strohmayer G. 2003 *Plasma Phys. Control. Fusion* **45** 1523
[4] Raffray A.R. *et al* 2010 *Fusion Eng. Des.* **85** 93
[5] Sizyuk V. and Hassanein A. 2010 *Nucl. Fusion* **50** 115004
[6] Sizyuk V., Hassanein A. and Sizyuk T. 2006 *J. Appl. Phys.* **100** 103106
[7] Hassanein A. and Sizyuk T. 2013 *Phys. Plasmas* **20** 053105
[8] Sizyuk V., Hassanein A., Morozov V. and Sizyuk T. 2006 *Report* No ANLMCS-CPH-06/56, Argonne National Laboratory
[9] Sizyuk V. and Hassanein A. 2013 *Nucl. Fusion* **53** 073023
[10] Sizyuk T. and Hassanein A. 2012 *Phys. Plasmas* **19** 083102
[11] Hassanein A., Kulcinski G.L. and Wolfer W.G. 1984 *Nucl. Eng. Des. Fusion* **1** 307
[12] Hassanein A. *et al* 2006 *EUV Sources for Lithography* ed V. Bakshi (Bellingham, WA: SPIE) p 277 chapter 9
[13] Hassanein A., Sizyuk V., Sizyuk T. and Harilal S.S. 2009 *J. Micro/Nanolithogr. MEMS MOEMS* **8** 041503
[14] Tolkach V., Morozov V. and Hassanein A. 2002 *Report* No ANL-ET/02-23, Argonne National Laboratory
[15] Hassanein A. and Konkashbaev I. 2003 *J. Nucl. Mater.* **313–316** 664
[16] Hassanein A., Sizyuk V. and Sizyuk T. 2011 *IEEE Trans. Plasma Sci.* **39** 2880
[17] Hassanein A., Sizyuk V., Miloshevsky G. and Sizyuk T. 2013 *J. Nucl. Mater.* **438** S1266
[18] Cabalin L.M. and Laserna J.J. 1998 *Spectrochim. Acta* B **53** 723
[19] Harilal S.S., Bindhu C.V., Issac R.C., Nampoori V.P.N. and Vallabhan C.P.G. 1997 *J. Appl. Phys.* **82** 2140
[20] Gojani A.B., Yoh J.J. and Yoo J.H. 2008 *Appl. Surf. Sci.* **255** 2777